Current Biology 23, 2140–2145, November 4, 2013 ©2013 Elsevier Ltd All rights reserved http://dx.doi.org/10.1016/j.cub.2013.08.054

Report

# Quantitative Imaging of Transcription in Living *Drosophila* Embryos Links Polymerase Activity to Patterning

Hernan G. Garcia,[1] Mikhail Tikhonov,[1,2] Albert Lin,[1] and Thomas Gregor[1,2,*]
[1]Joseph Henry Laboratories of Physics, Princeton University, Princeton, NJ 08544, USA
[2]Lewis-Sigler Institute for Integrative Genomics, Princeton University, Princeton, NJ 08544, USA

## Summary

**Spatiotemporal patterns of gene expression are fundamental to every developmental program. The resulting *macroscopic* domains have been mainly characterized by their levels of gene products [1–3]. However, the establishment of such patterns results from differences in the dynamics of *microscopic* events in individual cells such as transcription. It is unclear how these microscopic decisions lead to macroscopic patterns, as measurements in fixed tissue cannot access the underlying transcriptional dynamics [4–7]. In vivo transcriptional dynamics have long been approached in single-celled organisms [8–12], but never in a multicellular developmental context. Here, we directly address how boundaries of gene expression emerge in the *Drosophila* embryo by measuring the absolute number of actively transcribing polymerases in real time in individual nuclei. Specifically, we show that the formation of a boundary cannot be quantitatively explained by the rate of mRNA production in each cell, but instead requires amplification of the dynamic range of the expression boundary. This amplification is accomplished by nuclei randomly adopting active or inactive states of transcription, leading to a collective effect where the fraction of active nuclei is modulated in space. Thus, developmental patterns are not just the consequence of reproducible transcriptional dynamics in individual nuclei, but are the result of averaging expression over space and time.**

## Results

To monitor the transcriptional dynamics that lead to the formation of these boundaries, we have adapted a technique from single-celled organisms [8–12] that has been previously used to track mRNA in fly embryos [13]. Our technique allows for in vivo monitoring of nascent mRNA transcripts using a DNA sequence that upon transcription forms an mRNA stem loop. Cassettes with multiple copies of the stem loop are bound specifically by a constitutively expressed protein fused to GFP resulting in spatially localized fluorescence (Figure 1A).

Using this technique, we examine the step-like expression of the Bicoid (Bcd) activated *hunchback* (*hb*) P2 enhancer and promoter (Figures S1A and S1B available online), one of the best-studied expression patterns in the fly embryo [14, 15]. The P2 enhancer is one of three enhancers involved in the establishment of the endogenous *hb* pattern [16]. Reporter constructs for the P2 enhancer constitute an easily accessible model for the formation of developmental patterns in general, rather than reflecting on endogenous pattern formation. We drive the expression of a *lacZ* reporter gene with the mRNA stem loops located at its 5′ end (Figure 1A). Approximately 5 min into the ninth round of nuclear division, nuclear cycle (n.c.) 9, fluorescent spots associated with nuclei emerge within the syncytial blastoderm (Figure 1B). We detect single peaks of fluorescence activity during well-defined time windows that are synchronous with the rapid nuclear cycles in the early embryo (Movie S1). In n.c. 14, the expected step in zygotic expression is apparent in a surface layer of cells along the ~500 μm long axis of the embryo (Figure 1C). The bright spots are sites of nascent transcript formation, as confirmed by mRNA fluorescence in situ hybridization (FISH) [17]. Their fluorescence is directly proportional to the number of actively transcribing polymerase molecules (Figures S2A and S2B). Thus, we extract fluorescent traces reflecting transcriptional activity in individual nuclei as a function of space and time (Figures 1D and S2C–S2G).

To validate that these fluorescence dynamics faithfully recapitulate actual transcription, we measure the rate of transcript elongation in live embryos. This is accomplished by using an additional reporter construct in which the MS2 stem loops are located at the 3′ end of the *lacZ* gene, instead of the 5′ end. Upon entering a n.c., the onset of expression of the 3′ construct shows a clear delay with respect to the 5′ one (Figure 2A and Movie S2). The time delay measured over multiple embryos yields a rate of elongation $r_{elongation}$ = 1.54 ± 0.14 kb/min (Figure 2A). Measurements performed in *Drosophila* cell culture and in fixed embryos of 1.1–1.5 kb/min [18] are in agreement with our approach, suggesting that our technique gives direct access to the underlying transcriptional dynamics.

To connect the dynamics of transcription initiation (5′ signal) to the dynamics of transcription termination (3′ signal), we compare the fluorescent traces obtained with the two constructs in n.c. 14 (Figure 2B). Given the difference in construct geometry (see the Supplemental Experimental Procedures) and the same rate of polymerase loading, the overall signal of the 5′ construct should contain 3.6 times more labeled mRNA molecules than the 3′ construct. A deviation from 3.6 would indicate that not all initiated mRNA molecules are terminated and are possibly aborted during elongation. We find a ratio between the maximum polymerase loading of both signals of 3.3 ± 0.5, consistent with the majority of mRNA molecules being transcribed to termination. Therefore the dynamics of the larger 5′ signal can be used as a proxy for the production of full transcripts.

We link the transcriptional dynamics of the 5′ construct to the emergence of the macroscopic pattern, whose formation results from the accumulation of cytoplasmic mRNA transcripts with a half-life of over 3 hr [19] (in comparison, endogenous *hb* transcripts are stable for ~60 min [17]). This accumulation of mRNA is estimated by integration of the fluorescence traces of individual transcription spots over time (Figure S3A). We recover the spatial profile by averaging these integrated traces over nuclei in bins of 2.5% egg length (EL) along the anterior-posterior (AP) axis (Figures 3A, S3A, and

*Correspondence: tg2@princeton.edu

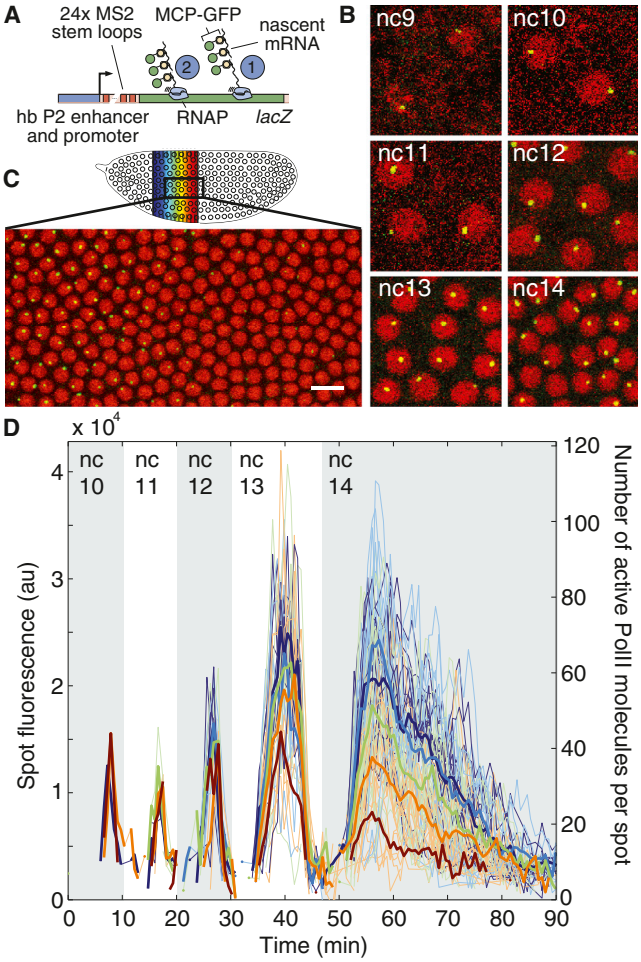


Figure 1. In Vivo Tracking of Transcriptional Activity using mRNA Stem Loops

(A) The *hb* P2 enhancer controlling the *hb* P2 promoter transcribes a *lacZ* gene with 24 MS2 stem loops located at its 5′ end. The MCP-GFP protein that binds to the stem loops is provided maternally.

(B) Snapshots (26 × 26 $\mu m^2$) of the anterior region of an embryo expressing the MS2-MCP system in nuclear cycles 9 through 14, showing MCP-GFP (green) and Histone-RFP (red) fluorescence. Brightness and contrast of each time point were adjusted independently.

(C) Typical field of view of an embryo between 30%–50% egg length (EL), anterior facing left. The scale bar represents 10 $\mu m$. See also Movie S1.

(D) Fluorescence traces corresponding to individual spots of transcription (thin lines) color-coded by their nuclear position along the embryo as shown in (B) and corresponding mean fluorescence over position-binned nuclei (thick lines).

See also Figure S1 and Movie S1.

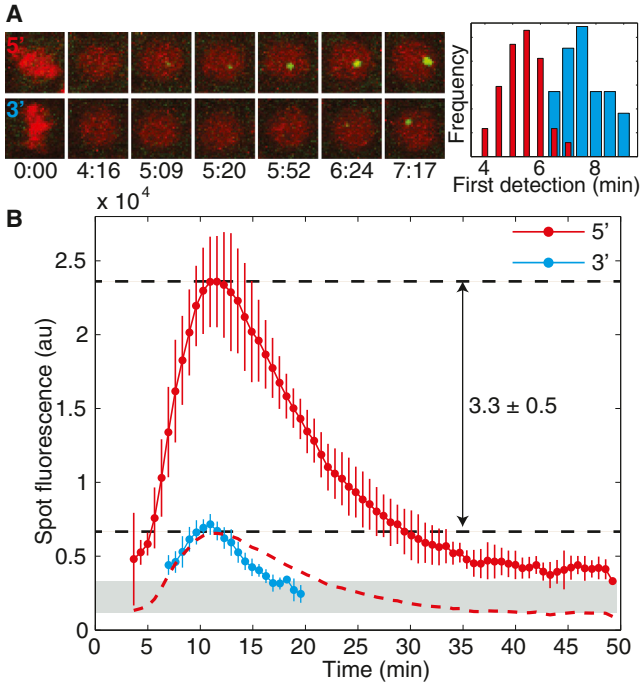


Figure 2. Rate of Transcript Elongation and Dynamics of Initiation and Termination

(A) Comparison of expression dynamics of a single allele of the enhancer-construct in two nuclei (different embryos) with stem loops located at the 5′ end and the 3′ end of the *lacZ* gene, respectively. Images (7 × 7 $\mu m^2$) show Histone-RFP (red) and MCP-GFP (green) fluorescence; time 0 min corresponds to anaphase 13. The histogram shows the distribution of times of first spot detection. The difference of the distribution means (i.e., 5.4 ± 0.1 min [red] and 7.6 ± 0.2 min [blue]) is used to measure the rate of transcript elongation $r_{elongation}$ = 1.54 ± 0.14 kb/min (difference between 5′ and 3′ stem loop locations is 3.4 kb; errors are propagated from the SE of the distributions; number of nuclei, $n_{5'}$ = 34 and $n_{3'}$ = 22).

(B) Average fluorescence in n.c. 14 as measured by the 5′ and 3′ constructs. The ratio between the maximum 5′ and 3′ fluorescence level is 3.3 ± 0.5, consistent with the predicted ratio of 3.6 based on gene length. The red dashed line is the 5′ signal rescaled by 3.6. The gray bar is the estimated detection limit of 6 ± 3 nascent mRNA molecules per spot (Figure S2H and Movie S2).

See also Figures S2 and S3 and Movie S2.

S3B). Comparison of this spatial profile to that obtained by FISH counts of cytoplasmic transcripts confirms that the patterns obtained with both methods are comparable within experimental error (Figures S3D–S3H).

mRNA FISH also provides a control for the behavior of our construct in terms of absolute counts of mRNA molecules. We count an absolute number of (220 ± 20) molecules produced per nucleus in the anterior region during n.c. 13 (Figures S3D–S3H). Assuming uniform polymerase loading on the gene and that each fluorescent spot contains two replicated sister chromatids [17, 20], this number corresponds to an average spacing of 150 ± 30 bp per gene, and a loading rate of one molecule every 6 ± 1 s per promoter. These results are consistent with absolute counts of endogenous *hb* mRNA and the maximum estimated rate of polymerase loading in fixed embryos [17, 21]. These numbers allow us to calibrate the integrated profile (Figure 3A) and the fluorescent traces (Figure 1D) in terms of the absolute number of mRNA molecules produced and the number of actively transcribing polymerase molecules, respectively (Figure S3H).

Developmental boundaries are characterized by the width of their transition region and their dynamic range of expression (Figure 3A and S1B). The width determines the spatial resolution of adjacent developmental states [3, 22], while a large dynamic range allows for deterministic downstream decisions [23, 24]. Our obtained spatial profile displays a first clear sign of a boundary during n.c. 13. The width of the transition does not change significantly between n.c. 13 (21% ± 2% EL) and n.c. 14 (20% ± 2% EL). On the other hand, the dynamic range of the boundary changes noticeably between n.c. 13 and n.c. 14 from 5.8 ± 0.8 to 26 ± 2 (Figure 3A), as confirmed by *lacZ*-mRNA FISH (Figure S3H).

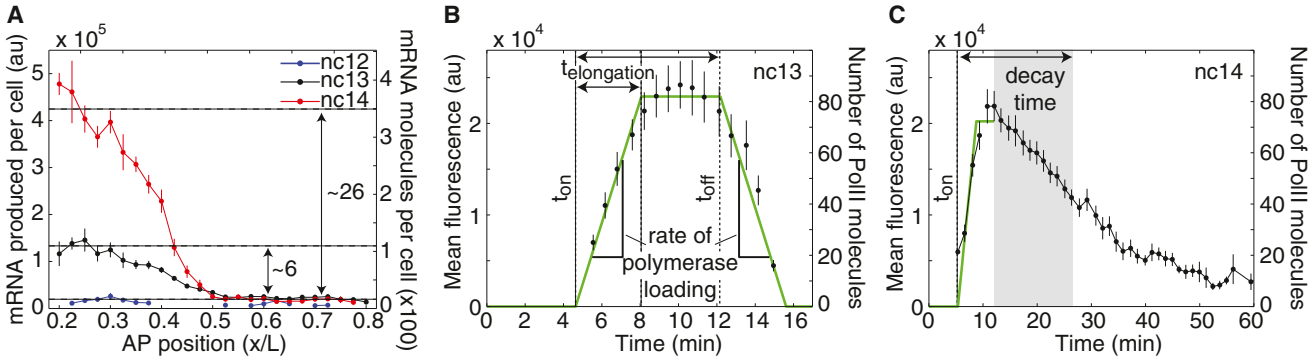


Figure 3. Dynamics of Boundary Formation

(A) Total amount of mRNA produced as a function of AP position for n.c. 12 (blue; n = 13), n.c. 13 (black; n = 24), and n.c. 14 (red; n = 24) (see the main text and Figures S3A–S3C). mRNA production is normalized per equivalent n.c. 14 cell (i.e., the production per cell in n.c.12 and n.c. 13 is divided by four and two, respectively); error bars show the SE over multiple embryos. The dynamic range, defined as the ratio between maximum and minimum expression of the pattern (Figure S1B), is 5.8 ± 0.8 and 26 ± 2 for n.c. 13 and n.c. 14, respectively.

(B and C) Model of transcriptional dynamics: transcription is turned on at a time $t_{on}$ after mitosis with a constant rate of polymerase loading, resulting in a linear increase in fluorescence. After a time $t_{elongation}$ = 3.4 ± 0.3 min (i.e., the ratio between the length of the gene of 5.4kb and $r_{elongation}$), the first polymerase that was loaded will terminate transcription and leave the transcription site. A steady state of polymerase density (i.e., a stable fluorescence level) between newly loaded and terminating polymerases will persist until the promoter is turned off at $t_{off}$. Polymerase loading ceases, and the remaining polymerases terminate transcription at the reverse (negative) rate with which they were loaded. The difference between the turn off and turn on times defines the transcription time window (top arrows). The green curve shows a typical three-parameter fit to the mean fluorescence of nuclei located in a bin of size 2.5% EL centered around 30% EL in n.c. 13 (B) and n.c. 14 (C). In (C), only $t_{on}$ and the rate of polymerase loading are determined by the fit; for determination of $t_{off}$ in (C), see Figures S4A and S4B.

All errors show the SE over multiple nuclei. See also Figures S1 and S4.

Our live-imaging approach gives us the opportunity to determine the microscopic dynamics of transcription that lead to the formation of macroscopic pattern boundaries. The modulation of transcription along the AP axis is thought to determine the differential accumulation of gene product that ultimately generates the boundary (Figure S1B). Nuclei are expected to determine their rate of RNA polymerase (RNAP) loading based on the local concentration of the Bcd input gradient (Figures S1A and S1D) [2, 23, 25, 26]. Additionally, the window of time over which transcription occurs is modulated due to varying Bcd activator concentration during interphase (Figure S1C–S1E) [27]. In order to extract the rate of polymerase loading and the time window of active transcription at different positions along the AP axis, we use a simple effective model of transcription. In this model, the promoter becomes active at a time $t_{on}$ after mitosis and RNAP molecules are loaded at a constant rate. This effective rate is the combination of microscopic processes such as polymerase binding to the promoter, promoter-proximal pausing and its subsequent release. At a time $t_{off}$, the promoter is turned off and polymerase loading ceases, defining the window of time ($t_{off}$–$t_{on}$) over which transcription is active (Figures 3B and 3C). We find that the proposed model closely follows the average time trace of all active transcription sites within a given 2.5% EL region during n.c. 13 (Figure 3B). The equivalent traces during n.c. 14 follow similar initial dynamics, but display a slowly decreasing fluorescence signal (Figures 3C, S4A, and S4B). It is plausible that in n.c. 13 transcription initiation is being turned off by the decay in nuclear Bcd levels upon mitosis entry [27] or by mitotic repression [28]. In contrast, transcription in n.c. 14 shuts down an hour before any cell undergoes mitosis. This shutdown could be related to the presence of high gap gene expression levels at that stage whose repressive function overrules that of the Bcd activator [27, 29, 30].

By fitting our model to the data, we extract the rate of polymerase loading and the time window of transcription as a function of AP position (Figures S4F and S4G). As expected from the pattern of mRNA accumulation (Figures 3A and S1), the rate of polymerase loading in individual nuclei is modulated along the AP axis in a step-like manner (Figure 4A). Nuclei in the anterior region express at higher rates than nuclei in the posterior region, and the levels both in n.c. 13 and n.c. 14 are comparable. The average rate of polymerase loading in the posterior of the embryo is given by the basal activity of the reporter construct in the absence of the Bcd activator (Figures 4A and S5 and Movie S3). In contrast to the rate of polymerase loading, the window of time during which transcription is active displays only a moderate variation along the AP axis during n.c. 12 and 13 (Figures 4B and S4C–S4E). However, n.c. 14 shows a clear modulation in the transcription time window as a function of AP position with a dynamic range of 1.9 ± 0.1.

Are these two extracted parameters (i.e., the effective *rate of polymerase loading* and the *transcription time window*) sufficient to recover the measured total amount of mRNA? In our effective model of transcription and in the absence of any other regulatory mechanisms, the total amount of mRNA produced per nucleus (Figure 3A) should equal the product of these two extracted parameters (Figures 4A and 4B). Indeed, we find a reasonable agreement between the two curves in n.c. 13 (Figure 4C, green and black curves), indicating that the modulation of these two microscopic parameters is enough to explain the formation of the macroscopic pattern. However, in n.c. 14 the same approach fails to quantitatively reproduce the directly measured total amount of mRNA (Figure 4D, green and red curves). Combining dynamic ranges of 4.8 ± 0.2 (rate of polymerase loading; Figure 4A) and 1.9 ± 0.1 (time window; Figure 4B) is not enough to recover the observed 26- ± 2-fold dynamic range in n.c. 14. Therefore, an additional regulatory mechanism that serves as an amplifier

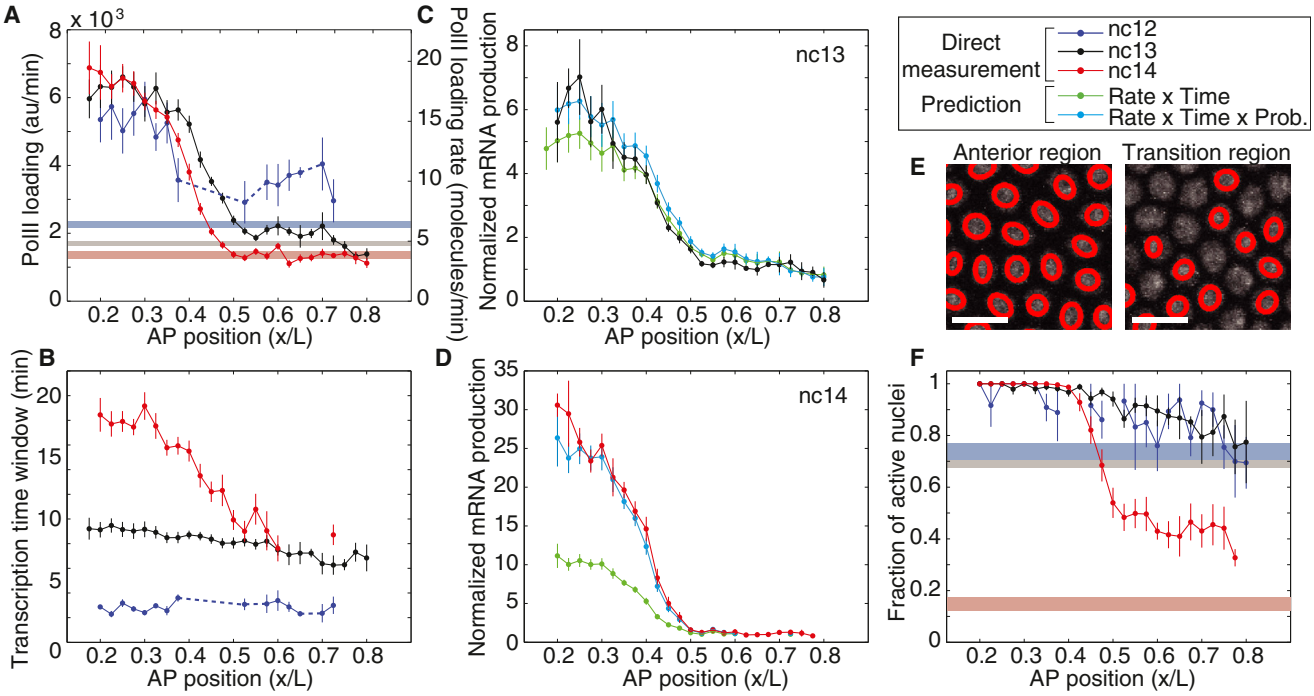


Figure 4. Formation of the Pattern Boundary Has Three Independent Dynamical Components

(A and B) Mean rate of polymerase loading (A) and mean window of time for transcription (B) as a function of position along the AP axis (for n.c. 12 [blue; n = 13 embryos], n.c. 13 [black; n = 24], and n.c. 14 [red; n = 24]; Figures S4A–S4E). Background values corresponding to a nonfunctional Bcd fly line are shown as horizontal bars using the same color coding (Figure S5 and Movie S3). See Figures S4F and S4G for a summary of transcription dynamics.

(C and D) mRNA produced as a function of AP position in n.c. 13 (C) and n.c. 14 (D). Data are normalized to the posterior end of the profiles. The direct measurement corresponds to the data shown in Figure 3A. Predictions (green and cyan) are obtained by multiplying the different values obtained in (A), (B), and (F).

(E) Representative fields of view (Histone-RFP) of nuclei in n.c. 14 in the activation (left, 29% EL) and transition regions (right, 61% EL). Nuclei where transcription was detected at any point over the entire n.c. are circled in red (Movies S4). Noncircled nuclei did not display any detectable transcription over the whole n.c. Scale bars represent 10 μm.

(F) Mean fraction of active nuclei as a function of position along the AP axis (Figure S6B). Color coding is as in (A) and (B).

In (A), (B), and (F), error bars show the SE over multiple embryos; in (C) and (D), error bars in the predictions are obtained by propagating the errors from (A), (B), and (F). See also Figures S5 and S6 and Movies S3 and S4.

for the dynamic range of the final gene expression boundary is necessary.

The mechanism of this amplifier is revealed by quantifying the number of nuclei in which transcription is detected as a function of AP position. All nuclei anterior to the boundary show expression, whereas only a fraction of the posteriorly located nuclei display activity (Figure 4E and Movie S4). No transcription is detected in inactive nuclei at any time point in the cycle. In n.c. 12 and 13, the local fraction of active nuclei across the boundary is only moderately modulated (Figure 4F). However, a strong modulation in the fraction of active nuclei is observed in n.c. 14, with a dynamic range of 2.3 ± 0.1. Interestingly, the fraction of active nuclei at the posterior end, where vanishing concentrations of Bcd protein are present [26], is higher than the fraction of active nuclei in the absence of Bcd (Figures 4F and S5D). This might indicate a uniform Bcd-dependent change in overall capacity of nuclei to transcribe. Moreover, we observe no preference for inactive n.c. 13 nuclei to divide into inactive daughter nuclei in n.c. 14, indicating that the state of nuclear activity is not transmitted through mitosis 13 (Figure S6A).

The switching of nuclei in n.c. 14 is independent of the control of the rate of polymerase loading. First, although the profile of the rate of polymerase loading is comparable in n.c. 13 and 14 (Figure 4A), the control of the fraction of active nuclei only becomes relevant in n.c. 14 (Figure 4F). This behavior indicates an overall change in transcription leading to the onset of the regulation of nuclear activity. Second, the rate of polymerase loading and the fraction of active nuclei present significantly different spatial patterns in n.c. 14 (Figure S6B), suggesting that they are distinct consequences of the input activator. Finally, lack of detection of active nuclei in n.c. 14 is not due to a substantial fraction of fluorescent spots falling below our detection limit. We estimate our systematic error to be less than 5%, well below the detected modulation in the fraction of active nuclei (Figure S2I).

Adding regulation of nuclear activity to our model leads to a good agreement between the directly measured total amount of mRNA produced and the product of the three dynamic parameters (Figure 4D, cyan and red curves), i.e., the *rate of polymerase loading*, the *transcription time window*, and the *fraction of active nuclei*. The random patches of active and inactive nuclei along the boundary (Figure 4E and Movie S4) eventually lead to a final smooth cytoplasmic mRNA profile (Figure S3H), suggesting that averaging at the level of cytoplasmic mRNA both in space and time is required [17, 23]. Therefore, it is these three basic microscopic features of transcriptional dynamics that are both necessary and sufficient to describe the formation of the macroscopic boundary.

## Discussion

In multicellular organisms the formation of macroscopic patterns is believed to be the result of dynamical decisions made in individual cells [23, 31]. However, this relation cannot be tested using available fixed-tissue techniques, as they are unable to directly report on the dynamics of transcription. By monitoring transcriptional dynamics in living embryos we demonstrate that the formation of a pattern boundary can only be partially described by the modulation of the rate of polymerase loading and the time window of transcription (Figure 4D). The large dynamic range of developmental transcription boundaries is only recovered when the extra regulation of stochastic nuclear activity is added. Cytoplasmic mRNA patterns result from the average production of active nuclei over space and time. Such a regulatory strategy is not restricted to a syncytial blastoderm, where all nuclei share a common cytoplasm. In the presence of membranes, activated cells could still secrete signaling molecules in order to reach a similar spatiotemporal averaging of the output [32, 33].

Based on fixed tissue experiments, it has been suggested that the presence of nuclei with random activation states is related to various mechanisms of transcriptional precision [6, 7]. However, we were able to shed light on the role of this regulation in the formation of patterns in the early *Drosophila* embryo only through direct live imaging of nuclear activity. For example, it was unclear whether stochastic transcription corresponds to nuclei turning on and off repeatedly or whether it results from nuclei not turning on at all over the whole nuclear cycle. Here, we provide evidence for the latter scenario. Furthermore, this mechanism has no clear analog in single-cell systems, and its molecular basis remains unclear. The fact that it occurs only during n.c. 14, but not in any of the previous cycles, suggests that its onset may be related to the midblastula transition (MBT) [34]. MBT marks the large-scale activation of the zygotic genome resulting in the presence of additional factors such as gap genes and repressor gradients that can change the regulatory landscape [2, 35–37]. In fact, posterior repressor gradients have been suggested to play a key role in the establishment of boundaries and could be responsible for the observed stochastic inactivation of nuclear activity [37]. A systematic screen in mutant backgrounds will be required in order to uncover which molecular species is responsible for this stochastic regulation.

Our quantification of the dynamics of transcriptional regulation and of its relationship to pattern formation exemplifies the level of genetic and quantitative control available in the fly embryo. This approach can be extended to other reporter constructs and to endogenous genes in *Drosophila* and in other multicellular organisms. In particular, it will be interesting to determine how the dynamics of the wild-type *hb* boundary compares to the dynamics observed in the context of the simple construct addressed in this work.

### Experimental Procedures

Female virgins maternally expressing MCP-GFP and Histone-RFP were crossed with males of the reporter line. Collected embryos were imaged using two-photon microscopy [26]. At each time point, a stack of ten images separated by 1 μm was acquired. MCP-GFP spots are detected and quantified in 3D [17] and assigned to the closest segmented nucleus. All animal usage is under the approval of Princeton University's Institutional Animal Care and Use Committee.

For details on transgenic fly construction, sample preparation, and data acquisition and analysis for both live imaging and mRNA FISH, please refer to the Supplemental Experimental Procedures.

### Supplemental Information

Supplemental Information includes Supplemental Experimental Procedures, six figures, and four movies and can be found with this article online at http://dx.doi.org/10.1016/j.cub.2013.08.054.

### Acknowledgments

We thank S. Blythe, E. Cox, S. Di Talia, L. Gavis, T. Idema, S. Little, R. Phillips, T. Schüpbach, A. Sgro, and E. Wieschaus for helpful discussions and comments on the manuscript. This work was supported by NIH grants P50 GM071508 and R01 GM097275, by a Princeton Dicke Fellowship (H.G.G.), and by Searle Scholar Award 10-SSP-274 (T.G.).

Received: July 26, 2013
Revised: August 23, 2013
Accepted: August 28, 2013
Published: October 17, 2013

### References

1. Poustelnikova, E., Pisarev, A., Blagov, M., Samsonova, M., and Reinitz, J. (2004). A database for management of gene expression data in situ. Bioinformatics *20*, 2212–2221.
2. Jaeger, J., Surkova, S., Blagov, M., Janssens, H., Kosman, D., Kozlov, K.N., Manu, Myasnikova, E., Vanario-Alonso, C.E., Samsonova, M., et al. (2004). Dynamic control of positional information in the early Drosophila embryo. Nature *430*, 368–371.
3. Dubuis, J.O., Samanta, R., and Gregor, T. (2013). Accurate measurements of dynamics and reproducibility in small genetic networks. Mol. Syst. Biol. *9*, 639.
4. Paré, A., Lemons, D., Kosman, D., Beaver, W., Freund, Y., and McGinnis, W. (2009). Visualization of individual Scr mRNAs during Drosophila embryogenesis yields evidence for transcriptional bursting. Curr. Biol. *19*, 2037–2042.
5. McHale, P., Mizutani, C.M., Kosman, D., MacKay, D.L., Belu, M., Hermann, A., McGinnis, W., Bier, E., and Hwa, T. (2011). Gene length may contribute to graded transcriptional responses in the Drosophila embryo. Dev. Biol. *360*, 230–240.
6. Perry, M.W., Boettiger, A.N., and Levine, M. (2011). Multiple enhancers ensure precision of gap gene-expression patterns in the Drosophila embryo. Proc. Natl. Acad. Sci. USA *108*, 13570–13575.
7. Lagha, M., Bothma, J.P., Esposito, E., Ng, S., Stefanik, L., Tsui, C., Johnston, J., Chen, K., Gilmour, D.S., Zeitlinger, J., and Levine, M.S. (2013). Paused Pol II coordinates tissue morphogenesis in the Drosophila embryo. Cell *153*, 976–987.
8. Bertrand, E., Chartrand, P., Schaefer, M., Shenoy, S.M., Singer, R.H., and Long, R.M. (1998). Localization of ASH1 mRNA particles in living yeast. Mol. Cell *2*, 437–445.
9. Golding, I., Paulsson, J., Zawilski, S.M., and Cox, E.C. (2005). Real-time kinetics of gene activity in individual bacteria. Cell *123*, 1025–1036.
10. Yunger, S., Rosenfeld, L., Garini, Y., and Shav-Tal, Y. (2010). Single-allele analysis of transcription kinetics in living mammalian cells. Nat. Methods *7*, 631–633.
11. Larson, D.R., Zenklusen, D., Wu, B., Chao, J.A., and Singer, R.H. (2011). Real-time observation of transcription initiation and elongation on an endogenous yeast gene. Science *332*, 475–478.
12. Lionnet, T., Czaplinski, K., Darzacq, X., Shav-Tal, Y., Wells, A.L., Chao, J.A., Park, H.Y., de Turris, V., Lopez-Jones, M., and Singer, R.H. (2011). A transgenic mouse for in vivo detection of endogenous labeled mRNA. Nat. Methods *8*, 165–170.
13. Forrest, K.M., and Gavis, E.R. (2003). Live imaging of endogenous RNA reveals a diffusion and entrapment mechanism for nanos mRNA localization in Drosophila. Curr. Biol. *13*, 1159–1168.
14. Driever, W., and Nüsslein-Volhard, C. (1989). The bicoid protein is a positive regulator of hunchback transcription in the early Drosophila embryo. Nature *337*, 138–143.
15. Margolis, J.S., Borowsky, M.L., Steingrímsson, E., Shim, C.W., Lengyel, J.A., and Posakony, J.W. (1995). Posterior stripe expression of

hunchback is driven from two promoters by a common enhancer element. Development *121*, 3067–3077.
16. Perry, M.W., Bothma, J.P., Luu, R.D., and Levine, M. (2012). Precision of hunchback expression in the Drosophila embryo. Curr. Biol. *22*, 2247–2252.
17. Little, S.C., Tikhonov, M., and Gregor, T. (2013). Precise developmental gene expression arises from globally stochastic transcriptional activity. Cell *154*, 789–800.
18. Ardehali, M.B., and Lis, J.T. (2009). Tracking rates of transcription and splicing in vivo. Nat. Struct. Mol. Biol. *16*, 1123–1124.
19. Thomsen, S., Anders, S., Janga, S.C., Huber, W., and Alonso, C.R. (2010). Genome-wide analysis of mRNA decay patterns during early Drosophila development. Genome Biol. *11*, R93.
20. Shermoen, A.W., McCleland, M.L., and O'Farrell, P.H. (2010). Developmental control of late replication and S phase length. Curr. Biol. *20*, 2067–2077.
21. O'Brien, T., and Lis, J.T. (1991). RNA polymerase II pauses at the 5′ end of the transcriptionally induced Drosophila hsp70 gene. Mol. Cell. Biol. *11*, 5285–5290.
22. Crauk, O., and Dostatni, N. (2005). Bicoid determines sharp and precise target gene expression in the Drosophila embryo. Curr. Biol. *15*, 1888–1898.
23. Gregor, T., Tank, D.W., Wieschaus, E.F., and Bialek, W. (2007). Probing the limits to positional information. Cell *130*, 153–164.
24. Yu, D., and Small, S. (2008). Precise registration of gene expression boundaries by a repressive morphogen in Drosophila. Curr. Biol. *18*, 868–876.
25. Rosenfeld, N., Young, J.W., Alon, U., Swain, P.S., and Elowitz, M.B. (2005). Gene regulation at the single-cell level. Science *307*, 1962–1965.
26. Liu, F., Morrison, A.H., and Gregor, T. (2013). Dynamic interpretation of maternal inputs by the Drosophila segmentation gene network. Proc. Natl. Acad. Sci. USA *110*, 6724–6729.
27. Gregor, T., Wieschaus, E.F., McGregor, A.P., Bialek, W., and Tank, D.W. (2007). Stability and nuclear dynamics of the bicoid morphogen gradient. Cell *130*, 141–152.
28. Shermoen, A.W., and O'Farrell, P.H. (1991). Progression of the cell cycle through mitosis leads to abortion of nascent transcripts. Cell *67*, 303–310.
29. Jaeger, J. (2011). The gap gene network. Cell. Mol. Life Sci. *68*, 243–274.
30. Liu, J., and Ma, J. (2013). Uncovering a dynamic feature of the transcriptional regulatory network for anterior-posterior patterning in the Drosophila embryo. PLoS ONE *8*, e62641.
31. Davidson, E.H. (2006). The Regulatory Genome: Gene Regulatory Networks in Development and Evolution (Burlington: Academic Press).
32. Lewis, J. (2008). From signals to patterns: space, time, and mathematics in developmental biology. Science *322*, 399–403.
33. Lander, A.D. (2013). How cells know where they are. Science *339*, 923–927.
34. Tadros, W., and Lipshitz, H.D. (2009). The maternal-to-zygotic transition: a play in two acts. Development *136*, 3033–3042.
35. Ahmad, K., and Henikoff, S. (2001). Modulation of a transcription factor counteracts heterochromatic gene silencing in Drosophila. Cell *104*, 839–847.
36. Bai, L., Ondracka, A., and Cross, F.R. (2011). Multiple sequence-specific factors generate the nucleosome-depleted region on CLN2 promoter. Mol. Cell *42*, 465–476.
37. Chen, H., Xu, Z., Mei, C., Yu, D., and Small, S. (2012). A system of repressor gradients spatially organizes the boundaries of Bicoid-dependent target genes. Cell *149*, 618–629.